

Chapter 16

Multiaxial Fatigue Behaviour of SLM 18Ni300 Steel



R. Branco , J. D. Costa , J. A. M. Ferreira , C. Capela , F. Berto ,
and W. Macek 

Abstract Fatigue behaviour of SLM 18Ni300 steel under proportional bending-torsion loading is studied. The fatigue tests are conducted under pulsating loading conditions using tubular specimens with a transversal circular hole. Three ratios of the normal stress to shear stress are considered, namely $\sigma/\tau = 4$, $\sigma/\tau = 2$ and $\sigma/\tau = 4/3$. Crack initiation sites were found for two diametrically opposite points around the hole, whose locations are governed by the loading scenario. Crack angles at the early stage of growth were successfully predicted from the first principal direction at the nodes with maximum values of the first principal stress at the hole. Fatigue crack initiation life was estimated based on the SWT parameter, defined from uniaxial low-cycle fatigue tests performed for smooth standard specimens under fully reversed strain-controlled conditions. Overall, predicted lives are in agreement with the experiments.

Keywords Multiaxial fatigue · Bending-torsion · Notch effect · SWT parameter · Fatigue life prediction

16.1 Introduction

Maraging steels are a special class of advanced high-strength steels, widely used in aircraft, aerospace, military, offshore, subsea, tooling and moulding industries [1, 2].

R. Branco (✉) · J. D. Costa · J. A. M. Ferreira · C. Capela
CEMMPRE, Department of Mechanical Engineering, University of Coimbra, Coimbra, Portugal
e-mail: ricardo.branco@dem.uc.pt

C. Capela
Department of Mechanical Engineering, Instituto Politécnico de Leiria, ESTG, Leiria, Portugal

F. Berto
Department of Mechanical and Industrial Engineering, Norwegian University of Science and Technology, 7491 Trondheim, Norway

W. Macek
Faculty of Mechanical Engineering and Ship Technology, Gdańsk University of Technology, Gabriela Narutowicza 11/12, 80-233 Gdańsk, Poland

This special class of steels, whose microstructure is formed by a cubic martensitic matrix, is hardened by finely dispersed nanometer-sized precipitates of intermetallic compounds, resulting from a metallurgical reaction involving no carbon, which seriously hampers the movements of dislocations and, thereby, promotes strengthening by precipitation hardening processes [3, 4].

Because of their martensitic matrix, these materials require a rapid quench from the austenitic region to temperatures below the martensite start temperature, which makes them particularly suited for the selective laser melting technology [4, 5]. This fact can be explained by the small size of the melt pool that leads to very high cooling rates. On the other hand, the cyclic reheating experienced by the material may trigger the nucleation of hardening precipitates without the need of additional heat treatments [4]. Last but not least, the geometrically complex shapes and the relatively reduced quantities associated with the typical application areas are two other important requirements that can be met by this process [4–6].

Selective laser melting is a very popular but unequivocally complex technique for metal processing that creates fully functional components, directly from three-dimensional digital models, by successive deposition of thin layers of material [4, 7]. Due to the nature of this additive manufacturing process, products are prone to different types of anomalies (e.g. porosities, inclusions, voids, cavities, microcracks, shrinkage, lack of fusion, excessive roughness, etc.) increasing the uncertainty concerning the mechanical behaviour [8, 9]. Therefore, a good understanding of structural integrity under monotonic and cyclic loading is pivotal to extend the field of application as well as to develop more sophisticated products. Regarding the 18Ni300 maraging steel, there are no studies focused on multiaxial loading. Therefore, this paper aims at fulfilling this gap. The paper studies the fatigue behaviour of tubular geometries with a transversal hole subjected to proportional bending-torsion loading.

16.2 Materials and Methods

The material considered in this study was a 18Ni300 maraging steel produced by selective laser melting (SLM). Its chemical composition and its main mechanical properties are summarised in Tables 16.1 and 16.2 [9].

Table 16.1 Nominal chemical composition of the AISI 18Ni300 steel

C	Ni	Mn	Co	Mo	Ti	Al	Cr	P	Si	Mn	Fe
0.01	18.2	0.65	9.0	5.0	0.6	0.05	0.3	0.01	0.1	0.04	Bal

Table 16.2 Main mechanical properties of the AISI 18Ni300 steel

Density	Young's modulus	Tensile strength	Yield strength	Porosity
7.42 g/cm ³	168 GPa	1147 MPa	910 MPa	0.74%

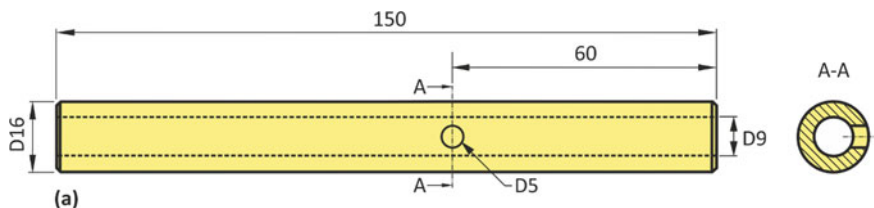


Fig. 16.1 Tubular specimen with a transversal circular hole fabricated via selective laser melting from 18Ni300 steel utilised in the multiaxial bending-torsion fatigue tests. Dimensions in millimetres

The specimen geometries, presented in Fig. 16.1, were fabricated in a vertical orientation, on the base plate, using a Concept Laser M3 linear printing system equipped with a Nd:YAG fibre laser. After the SLM process, specimens were machined at the external surface and polished to a scratch-free condition. The transversal hole was introduced by machining.

Fatigue tests were conducted using a DARTEC servo-hydraulic machine connected to a custom-made gripping system under proportional bending-torsion with a stress ratio (R) equal to 0. Three normal stress to shear stress (σ/τ) ratios were used, more precisely: $\sigma/\tau = 4$, $\sigma/\tau = 2$ and $\sigma/\tau = 4/3$. The nominal normal stress amplitudes varied between 78 and 96 MPa.

The evaluation of the stress and strain states at the notch vicinity was done through a finite-element model. Figure 16.2 shows the structured mesh developed in this study. It was developed in a parametric manner, with 8-node brick finite elements, assuming a homogeneous, linear-elastic and isotropic behaviour. At the notch region, an ultrarefined mesh was introduced to better describe the stress-strain gradients. The

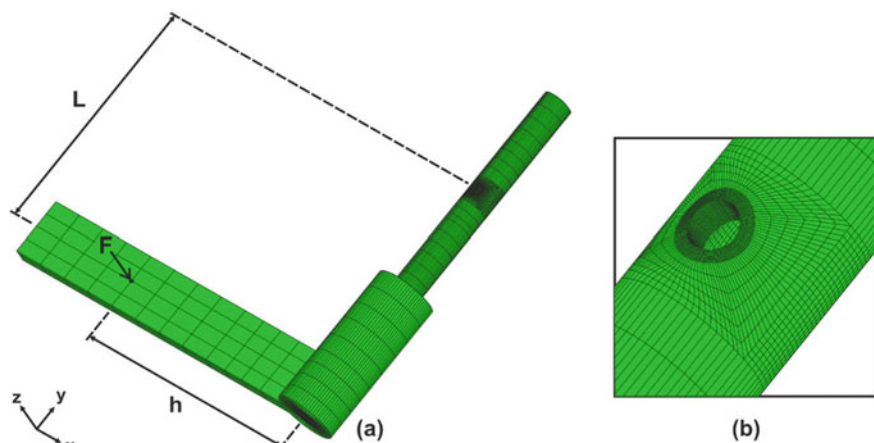


Fig. 16.2 Three-dimensional finite-element model developed in the present study: **a** Assembled mesh; and **b** hole region

assembled model contained 152,248 finite element and 163,138 nodes. The normal stress to shear stress ratios were defined using a single force (F) by adjusting its magnitude and its point of application. In this case, since L was fixed, the value of h , in the x -axis direction, was defined accordingly.

16.3 Results and Discussion

The fatigue process, in this geometry, is characterised by the initiation of two cracks at the hole in diametrically opposite points. Figure 16.3 shows an example for a test performed with $\sigma/\tau = 2$. In general, the experimental angles measured at the two sides, either α or β , are relatively similar, regardless of the normal stress to the shear stress ratio. The crack initiation angles, represented by β in Fig. 16.3, increased for lower σ/τ ratios, which is explained by the higher shear stress levels. Identical behaviour was found for the crack angles at the early stage of growth, represented in Fig. 16.4 by α . In this study, these angles were successfully predicted using the numerical model described above. Regarding the β angle, it can be reasonably estimated from the node with maximum value of the first principal stress. In relation to the α angle, it was determined by computing the first principal direction at the nodes with maximum value of the first principal stress. The good correlation between the experimental observations and the predicted values, either for the α angle or the β angle, is shown in Fig. 16.4. In order to simplify the analysis, scatter bands of $\pm 10^\circ$ and $\pm 5^\circ$ were added (dashed lines) in Fig. 16.4a, b, respectively. Overall, the average errors were 6.3° and 7.4° for β_1 and β_2 ; and 3.3° and 2.3° for α_1 and α_2 , respectively.

The examination of the fracture surfaces by scanning electron microscopy showed that crack initiation occurred from un-melted regions, most probably due to a lack of fusion or inadequate penetration (see Fig. 16.5). These heterogeneities, in the

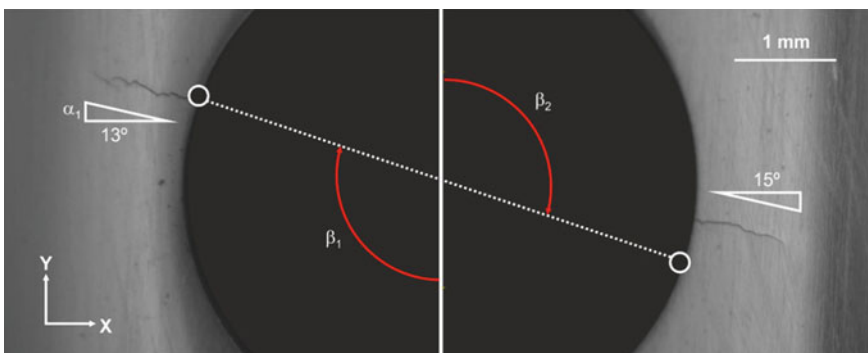


Fig. 16.3 Fatigue crack initiation sites observed experimentally for $\sigma/\tau = 2$ (α_1 and α_2 represent the angles on the left and right sides of the hole in accordance with the referential system of Fig. 16.2, and β_1 and β_2 represent the angles of the initiation sites measured in relation to the y -axis)

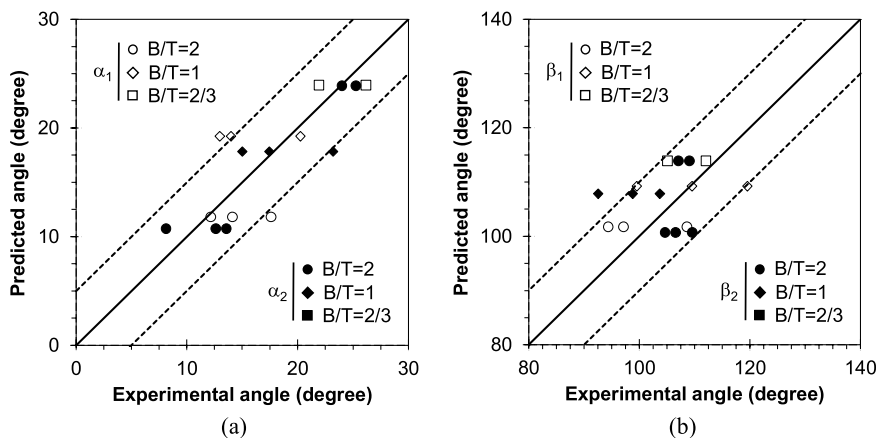


Fig. 16.4 Experimental observations versus predictions: **a** Crack initiation sites; and **b** crack angles at the early stage of growth

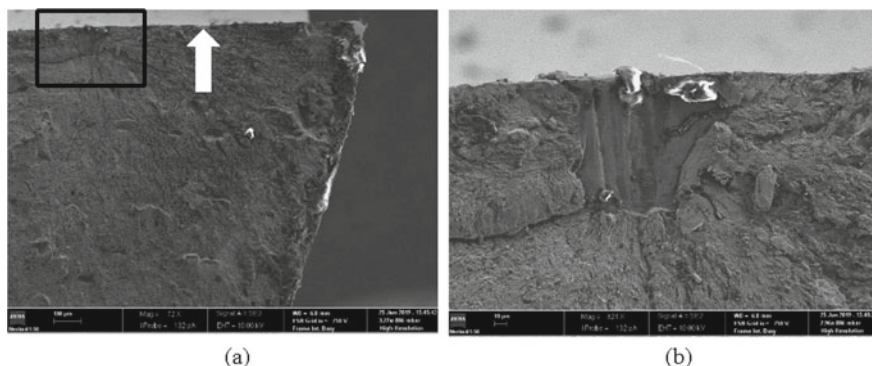


Fig. 16.5 Experimental observations versus predictions: **a** Crack initiation site; and **b** crack angle at the early stage of growth

presence of cyclic loads, created localised microscopic stresses, possibly larger than the yield stress, causing local plastic deformation and easing the fatigue crack initiation [10, 11]. Furthermore, it was also concluded that initiation occurred at the hole surface, near the outer diameter of the specimen (see Fig. 16.5a). This fact was corroborated by the numerical simulations. In Fig. 16.5a, the experimental initiation site, identified by the black box, and the predicted initiation site (based on the maximum value of the first principal stress) represented by the white arrow are compared. As can be seen, both locations are quite close, which is an interesting outcome.

Fatigue crack initiation life was predicted through a uniaxial model based on the SWT parameter [12]. It assumes two main premises [13]: (1) regardless of the geometric discontinuity, fatigue life is the same, if the stress–strain histories at the initiation sites are similar; and (2) fatigue failure occurs when a critical value of

damage is reached at the initiation site. Firstly, we develop a uniaxial damage law relating the SWT parameter (product of strain amplitude to maximum stress, see Eq. (16.1)) with the number of cycles to crack initiation (N_i). For this specific material, this law assumed the form:

$$SWT = \varepsilon_a \sigma_{\max} = 10^{1.5315} (N_f)^{-0.3567} \tag{16.1}$$

where ε_a is the strain amplitude, σ_{\max} is the maximum stress, and N_f is the number of cycles to failure. This power function was established from a series of low-cycle fatigue tests performed using smooth standard specimens under fully reversed strain-controlled conditions for strain amplitudes in the range ± 0.3 to $\pm 1.0\%$. The gauge section of these specimens had a diameter of 6 mm and a length of 19 mm. In a second stage, it is computed the fatigue crack initiation life (N_i) for the notched geometries. The modus operandi consists of four main steps (see Fig. 16.6): the multiaxial stress state is reduced to a uniaxial stress state at the notch-controlled process zone using the equivalent von Mises stress range (Fig. 16.6a); the local stress distribution is averaged by applying the Theory of Critical Distances (Fig. 16.6b); a representative hysteresis loop is generated by applying the equivalent strain energy density concept and the effective von Mises stress range computed in the previous step (Fig. 16.6c); and, finally, the corresponding value of the SWT parameter is inserted into the fatigue damage law to estimate the fatigue life (Fig. 16.6d). Here, the size of the notch-controlled process zone was estimated through the El-Haddad parameter (a_0):

$$a_0 = \frac{1}{\pi} \left(\frac{\Delta K_{th}}{\Delta \sigma_0} \right)^2 \tag{16.2}$$

where ΔK_{th} is the stress intensity factor range threshold, and $\Delta \sigma_0$ is the fatigue limit stress range. Based on previous studies, for $R = 0$, the former value is equal to $5.2 \text{ MPa m}^{0.5}$ and the latter was equal to 266 MPa [11, 14]. Therefore, $a_0 = 121.7 \text{ MPa}$.

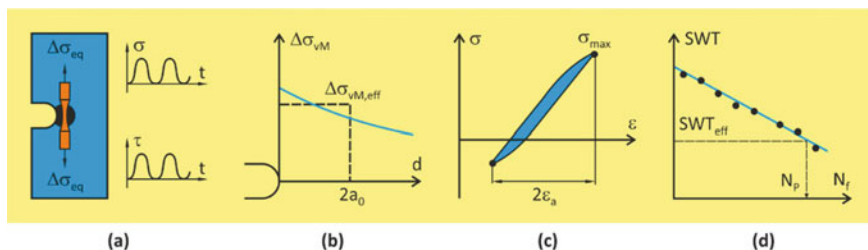
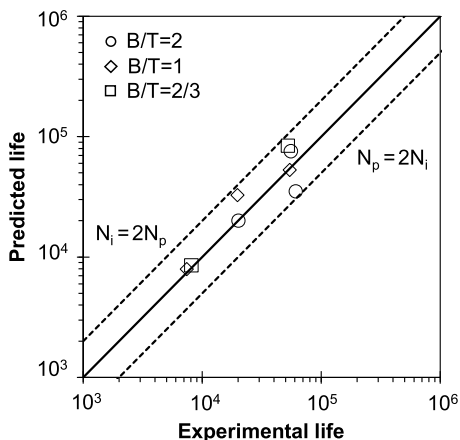


Fig. 16.6 Experimental observations versus predictions: **a** Crack initiation site; and **b** crack angle at the early stage of growth

Fig. 16.7 Experimental fatigue life versus predicted fatigue life for the multiaxial fatigue tests performed in the present study



The value of a_0 was used to estimate the experimental fatigue life. During the tests, the hole was observed periodically (interval ranging from 2000 to 5000 cycles, depending on the applied stress level) with a high-resolution camera to correlate the crack length with the number of cycles. Based on this information, we develop the so-called a - N curves (i.e. curves relating the crack length with the number of cycles). Then, these curves were fitted by exponential functions. The fatigue life was estimated, using the a - N curves, for a crack length equal to a_0 . Finally, the predicted fatigue lives (N_p) obtained by means of the procedure described above (see Fig. 16.6) were compared with those determined experimentally (N_i).

Figure 16.7 plots the experimental values against the predicted ones for the different loading scenarios studied in this paper. For the sake of clarity, scatter bands with factors of two were plotted (dashed lines), i.e. $2N_p = N_i$ and $2N_i = N_p$. Overall, the predictive capabilities of the proposed approaches are remarkable. In both cases, there is a strong correlation between the data, with all points within the delimited area. This clearly demonstrates the robustness of the proposed methodology. A close look at the figure shows a mixed behaviour; that is, predicted lives are either conservative or non-conservative. However, the data are very well correlated which is an interesting outcome.

16.4 Conclusions

This paper addressed the multiaxial fatigue behaviour of the 18Ni300 steel fabricated by selective laser melting. Tests were conducted under proportional bending-torsion loading for different normal stress to shear stress ratios using a tubular geometry with a transversal hole. A liner-elastic numerical model was developed to evaluate the stress and strain fields at the hole region. The following conclusions can be drawn:

- Fatigue failure was characterised by the initiation and growth of two cracks at diametrically opposite sites around the hole surface;
- Un-melted regions at the surface and sub-surface, resulting from insufficient fusion or inadequate penetration, were the cause of crack initiation;
- Fatigue crack initiation sites and fatigue crack angles at the early stage of growth were predicted from the principal stress field;
- The proposed fatigue life prediction model is suitable for SLM 18Ni300 components subjected to proportional bending-torsion loading.

Acknowledgment This research is sponsored by national funds through FCT - Fundação para a Ciência e a Tecnologia under the project UIDB/00285/2020.

References

1. Kempen K, Yasa E, Thijs L, Kruth JP, Van Humbeeck J (2011) Microstructure and mechanical properties of selective laser melted 18Ni-300 steel. In: *Physics procedia*
2. Kürsteiner P, Wilms MB, Weisheit A, Barriobero-Vila P, Jäggle EA, Raabe D (2017) Massive nanoprecipitation in an Fe-19Ni-xAl maraging steel triggered by the intrinsic heat treatment during laser metal deposition. *Acta Mater*
3. Mooney B, Kourousis KI, Raghavendra R (2019) Plastic anisotropy of additively manufactured maraging steel: Influence of the build orientation and heat treatments. *Addit Manuf*
4. Tan C, Zhou K, Ma W, Zhang P, Liu M, Kuang T (2017) Microstructural evolution, nanoprecipitation behavior and mechanical properties of selective laser melted high-performance grade 300 maraging steel. *Mater Des*
5. Jäggle EA, Choi PP, Van Humbeeck J, Raabe D (2014) Precipitation and austenite reversion behavior of a maraging steel produced by selective laser melting. *J Mater Res*
6. Zhu SP, He JC, Liao D, Wang Q, Liu Y The effect of notch size on critical distance and fatigue life predictions. *Mater Des* 196:109095
7. Suzuki A, Nishida R, Takata N, Kobashi M, Kato M (2019) Design of laser parameters for selectively laser melted maraging steel based on deposited energy density. *Addit Manuf*
8. Meneghetti G, Rigon D, Gennari C (2019) An analysis of defects influence on axial fatigue strength of maraging steel specimens produced by additive manufacturing. *Int J Fatigue*
9. Branco R, Costa JDM, Berto F et al (2018) Low-cycle fatigue behaviour of AISI 18Ni300 maraging steel produced by selective laser melting. *Metals (Basel)* 8(1)
10. Bajaj P, Hariharan A, Kini A, Kürsteiner P, Raabe D, Jäggle EA (2020) Steels in additive manufacturing: a review of their microstructure and properties. *Mater Sci Eng A*
11. Branco R, Silva J, Ferreira JM et al (2019) Fatigue behaviour of maraging steel samples produced by SLM under constant and variable amplitude loading. *Procedia Struct Integr*
12. Correia J, Apetre N, Arcari A et al (2017) Generalized probabilistic model allowing for various fatigue damage variables. *Int J Fatigue*
13. Branco R, Prates PA, Costa JD, Borrego LP, Berto F, Kotousov A, Antunes FV (2019) Rapid assessment of multiaxial fatigue lifetime in notched components using an averaged strain energy density approach. *Int J Fatigue* (2019)124:89–98. <https://doi.org/10.1016/j.ijfatigue.2019.02.005>
14. Santos LMS, Ferreira JAM, Jesus JS, Costa JM, Capela C (2016) Fatigue behaviour of selective laser melting steel components. *Theor Appl Fract Mech*